Measurements of the ^{128}Te(n, 2n)^{127m,g}Te reaction cross sections and isomeric cross section ratio of ^{127m,g}Te at the neutron energy of 14 MeV*

Junhua Luo (罗均华)[1,2†] Long He (贺龙)[3] Liang Zhou (周亮)[3] Li Jiang (蒋励)[4]

[1]Department of Basic Science, Lanzhou Institute of Technology, Lanzhou 730050, China
[2]Institute of New Energy, Hexi University, Zhangye 734000, China
[3]School of Physics and Electromechanical Engineering, Hexi University, Zhangye 734000, China
[4]Institute of Nuclear Physics and Chemistry, China Academy of Engineering Physics, Mianyang 621900, China

Abstract: In this study, measurements of the ^{128}Te(n, 2n)^{127m,g}Te reaction cross sections and the computation of the isomeric cross section ratio were performed around the neutron energy of 13−15 MeV. We used a γ-ray spectrometric technique to conduct the measurements. The neutron energy was produced by the ^{3}H(d,n)^{4}He reaction. For the ^{128}Te(n, 2n)^{127m,g}Te reaction, the excited state, ground state, total cross section, and isomeric cross section ratio were determined using the TALYS-1.96 code, a theoretical nuclear model that allows for variations in density options. The initial experimental data, assessed nuclear data, and theoretical calculations based on the TALYS-1.96 algorithm were compared with the measurement results. The new data produced by this study are essential for validating nuclear models and establishing parameters for nuclear reactions.

Keywords: ^{128}Te(n, 2n)^{127mg}Te reactions, activation method, secondary nuclear method, nuclear cross section, theoretical calculations with the TALYS-1.96

DOI: 10.1088/1674-1137/ad7370

I. INTRODUCTION

In nuclear reactions, the cross section data for residual nuclei states are vital [1−3]. Important parameters and test models for nuclear reactions can be derived from the data collected in previous studies [4, 5]. The large cross sections of the (n, 2n) reactions of different elements facilitate experimental measurements in the 14-MeV neutron energy region [6−9]. In addition, the spin cut-off factor can be determined using the (n, 2n) isomeric cross section ratio (a crucial approach) [10, 11]. However, measuring cross sections for the remaining nucleus states is challenging for a finite number of (n, 2n) reactions. For example, in the nuclear reaction ^{128}Te(n, 2n), the daughter nucleus decays, as shown in Fig. 1. The half-life ($T_{1/2}$=106.1 d) of the excited state (11/2$^-$) is much longer than that of the ground state (3/2$^+$, $T_{1/2}$=9.35 h), and it has no proper γ-ray with sufficient intensity. The characteristic rays have low energies and very weak intensities. Determining the efficiency of high-purity germanium (HP-Ge) detectors is challenging in regions of lower energy (E_γ<80 keV), as the absolute intensity is too small to count or measure. The results of the cross-sectional measurements of the ^{128}Te(n, 2n)^{127m}Te reaction are inconsistent and scarce because of the abovementioned reasons. Only four labs [12−15] have produced measurements from 630 to 949 mb, with a 50% difference. The ground states of the residual nucleus have characteristic rays at 417 and 360.3 keV, and using these values, researchers [12, 15] have determined the cross sections of the excited state (see Table 1). Other researchers have utilized both lines to determine the cross sections of the ground state [12, 13, 16−19]. Still other researchers [14, 20] have used beta counting or have discovered minimal information [21−23]. Various circumstances cause the cross sections of the nuclear reaction ^{128}Te(n, 2n)^{127g}Te to vary more than four times from 230 to 840 mb. The differences are mostly caused by three factors in the extensively researched 14-MeV neutron energy region, which are described as follows:

i. Issues with decay data (half-life and γ-ray intensity). The cross sections for the ^{128}Te(n, 2n)^{127m}Te reaction have been obtained by Lu *et al*. [12], Bormann *et al*. [14], and Zhou *et al*. [15] using a half-life of 109 d (see Table 1), and by Husain and Kuroda [13] using a half-life of 105 d. Recent measurements were performed for data using a half-life of 106.1 d [24]. Lu *et al*. [12], Husain and Kuroda [13], Schnabel *et al*. [16], Zhou *et al*. [17], Filatenkov *et al*. [18], and Filatenkov [19] determ-

Received 7 April 2024; Accepted 13 August 2024; Published online 14 August 2024
* Supported by the National Natural Science Foundation of China (12165006, 12375295)
† E-mail: luojh71@163.com

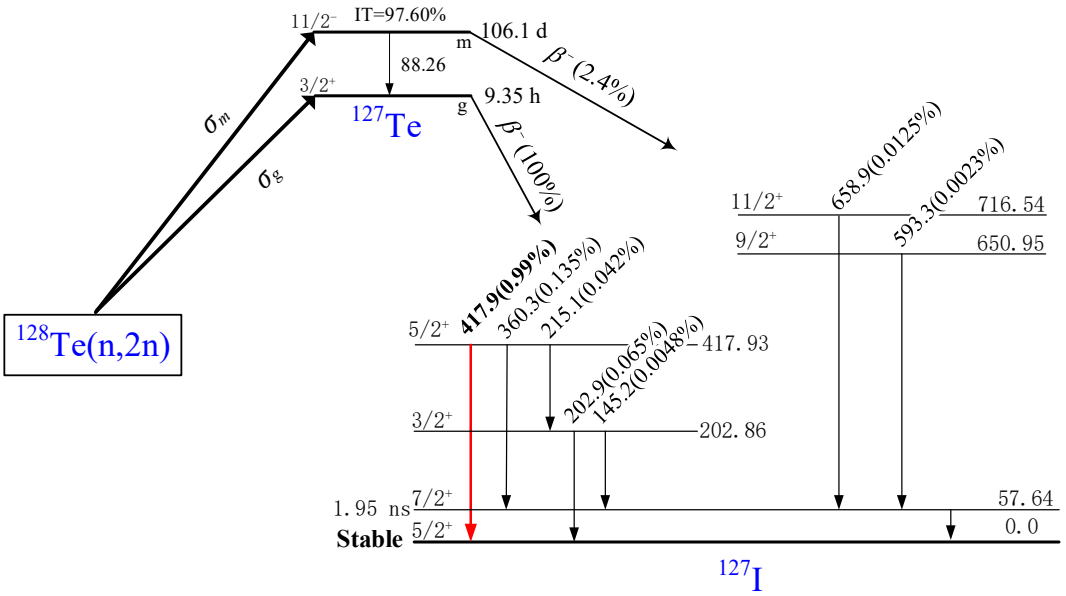

Fig. 1. (color online) The metastable and ground states formed by the ^{128}Te(n, 2n)^{127m,g}Te reaction [24].

Table 1. Cross-sectional measurements of the ^{128}Te(n, 2n)^{127m,g}Te reactions from reported measurements.

Reaction	Decay data	Detector	Monitor reaction	Reference
^{128}Te(n, 2n)^{127m}Te	$T_{1/2}$=109 d, $E\gamma$=417 keV, $I\gamma$=82%	GeLi	^{56}Fe(n,p)^{56}Mn	[12]
	$T_{1/2}$=105 d, decay data: *no information*	NaI	*No information*	[13]
	$T_{1/2}$=109 d, β counts	GEMUC	^{1}H(n,el)^{1}H	[14]
	$T_{1/2}$=109 d, $E\gamma$=360.3 keV, $I\gamma$=0.13464 %;	HPGe	^{93}Nb(n, 2n)^{92m}Nb	[15]
^{128}Te(n, 2n)^{127g}Te	$T_{1/2}$=9.4 h, $E\gamma$=417 keV, $I\gamma$= 0.83%	GeLi	^{56}Fe(n,p)^{56}Mn	[12]
	$T_{1/2}$=9.3 h, $E\gamma$=420 keV, $I\gamma$= 0.83%	NaI	*No information*	[13]
	$T_{1/2}$=9.48 h, β counts	GEMUC	^{1}H(n,el)^{1}H	[14]
	$T_{1/2}$=9.35 h, $E\gamma$=418.0 keV ($I\gamma$=0.993%), $E\gamma$=360.3 keV ($I\gamma$=0.135%)	HPGe	^{27}Al(n,α)^{24}Na	[16]
	$T_{1/2}$=9.35 h, $E\gamma$=417.9 keV, $I\gamma$= 0.99%	HPGe	^{93}Nb(n, 2n)^{92m}Nb	[17]
	$T_{1/2}$=9.35 h, $E\gamma$=417.9 keV, $I\gamma$= 0.99%		^{93}Nb(n, 2n)^{92m}Nb	[18]
	$T_{1/2}$=9.35 h, $E\gamma$=417.9 keV ($I\gamma$=0.99%), $E\gamma$=360.3 keV ($I\gamma$=0.135%)	GeLi	^{93}Nb(n, 2n)^{92m}Nb	[19]
	$T_{1/2}$=9.3 h, β counts	GeLi	*No information*	[20]
	$T_{1/2}$=9.3 h, decay data: *no information*	NaI	^{27}Al(n,α)^{24}Na	[21]
	$T_{1/2}$=9.3 h, enriched to 94.4 % of ^{128}Te, decay data: *No information*		^{130}Te(n, 2n)^{129g}Te	[22]
	$T_{1/2}$=9.5 h, decay data: *no information*	GEMUC	^{3}H(d,n)^{4}He	[23]

ined cross sections of the ^{128}Te(n, 2n)^{127g}Te reaction using γ-ray intensities of 0.83%, 0.83%, 0.993%, 0.99%, 0.99%, and 0.99%, respectively, for the same γ-ray energy of 417.9 keV. Recent measurements have used a γ-ray intensity of 0.99% [24].

ii. A variety of calculations. Previous researchers [12, 15] used the 417-keV and 306.3-keV gamma rays released in the ^{127g}Te decay to evaluate the reaction cross section of ^{128}Te(n, 2n)^{127m}Te [β^-(2.4%), IT(97.6%), $T_{1/2}$=106.1 d]. These two studies inconsistently calculated the cross sections of the excited state using the characteristic rays of the ground state (i.e., a secondary nuclear decay approach).

iii. Interfering reactions. For the ^{128}Te(n, 2n)^{127g}Te reaction, the characteristic rays are generated by the product nucleus ^{127g}Te and the ^{128}Te(n, 2n)^{127m}Te reaction via ^{127m}Te $\xrightarrow{\text{IT(97.6\%)}}$ ^{127g}Te (see Fig. 1). The interference of the excited state can be deduced through the isomeric transition. This is not discussed in detail in the early literature.

In this study, nuclear reaction cross section measurements were obtained via secondary nuclear decay for the

^{128}Te(n, 2n)^{127m}Te reactions. When the Te samples and Nb-based monitor foils were activated, the neutron flux and reaction cross section were measured. The remaining nuclear ground state characteristic rays (instead of low-energy rays) were used to quantify the nuclear reaction cross section σ_m of the excited states. The results indicated that the cross section σ_g of the pure ground state can be estimated using the residual nuclear decay technique. In addition, the isomeric cross section ratio of ^{127m,g}Te in the ^{128}Te(n, 2n) reaction was calculated. The uncertainty was carefully assessed based on the measurements. Finally, comparisons were made between the results obtained in this study and the early experimental and theoretical calculations that were derived from the TALYS-1.96 [25], ENDF/B-VIII.0 [26], BROND-3.1 [27], JEFF-3.3[28], JENDL-5[29], and TENDL-2021[30] assessment data.

II. CROSS SECTIONS OF THE EXCITED AND GROUND STATES

A. Excited state cross section

When the cooling time (t_1, see Fig. 2) is significantly longer than the half-life of the ground state (^{127g}Te) (typically greater than six half-lives), the characteristic rays of the ground state can be considered to originate entirely from the isomer transition of the excited state (^{127m}Te). This is based on the fact that the half-life of the product nucleus of the nuclear reaction ^{128}Te(n, 2n) is as shown in Fig. 1. Directly obtaining the cross section of the excited state from the characteristic ray activity of the ground state is possible using the following method.

The formula for the excited state cross section is [31]

$$\sigma_m = \frac{A_m C_{mg}(\lambda_g-\lambda_m)\lambda_m\lambda_g}{I_{\gamma g}\varepsilon_g M_m\eta_m K_m P_{mg}(\lambda_g^2 S_m D_m-\lambda_m^2 S_g D_g)} \times\left[\frac{I_\gamma\varepsilon\eta KMSD}{AC\lambda}\sigma\right]_{Nb}, \quad (1)$$

where the subscript Nb represents the term corresponding to the monitor reaction,

$$S_m = 1-\mathrm{e}^{-\lambda_m T},\quad S_g = 1-\mathrm{e}^{-\lambda_g T},$$
$$D_m = \mathrm{e}^{-\lambda_m t_1}-\mathrm{e}^{-\lambda_m(t_1+t_2)},\quad D_g = \mathrm{e}^{-\lambda_g t_1}-\mathrm{e}^{-\lambda_g(t_1+t_2)},$$

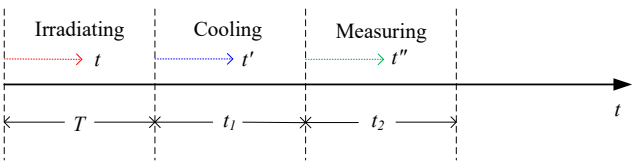

Fig. 2. (color online) Schematic illustration of the times in which the sample is irradiated, cooled, and measured.

and K is the neutron fluence fluctuation factor:

$$K = \left[\sum_i^L \Phi_i\left(1-\mathrm{e}^{-\lambda\Delta t_i}\right)\mathrm{e}^{-\lambda T_i}\right]/\Phi S. \quad (2)$$

B. Ground state cross section

When the cooling time is less than three times the half-life of the ground state, the isomer transition of the excited state affects the ground state, and the following equation can be used to calculate the ground state formation cross sections [32, 33]:

$$\sigma_g = \frac{[S\varepsilon I_\gamma\eta KMD]_{Nb}}{[S\varepsilon I_\gamma\eta KMD]_g}\cdot\frac{[\lambda AFC]_g}{[\lambda AFC]_{Nb}}\sigma_{Nb}. \quad (3)$$

Table 2 lists the significance of each quantity displayed in Equations (1)-(3). Table 3 lists the self-absorption correction factors of the measured characteristic 417.9-keV γ-ray corresponding to the five Te samples.

III. EXPERIMENTAL ANALYSIS

A. Samples and irradiations

Tellurium samples with a natural isotopic composi-

Table 2. Description of the symbols displayed in Eqs. (1)–(3).

Symbols	Physical significance
T	total irradiation time
t_1	total cooling time
t_2	total measurement time
A	atomic weight
C	measured full-energy peak area
$I\gamma$	gamma-ray intensity
M	mass of the sample
L	number of time intervals into which the irradiation time is divided
Δt_i	duration of the i-th time interval
T_i	time interval from the end of the i-th interval to the end of the irradiation time
F	coefficients reflecting self-absorption for the specific gamma-ray energy
σ	reaction cross section
λ	decay constant of the residual nucleus
ε	full-energy peak efficiency of the measured characteristic gamma ray
η	abundance of the target nuclide
Φ_i	neutron flux averaged over the sample during Δt_i
Φ	neutron flux averaged over the sample during the total irradiation time T

Table 3. Self-absorption correction factors for the five Te samples at the measured characteristic 417.9-keV gamma-ray energy. The angles of the five samples toward the beam are 0° (no. 1), 45° (no. 4), 90° (no. 2), 110° (no. 5), and 135° (no. 3).

Gamma-ray energy (keV)	μ/ρ (cm^2/g)	μ (cm^{-1})	Sample no.	Correction factor F
417.9	0.1122	0.700	1	1.069
			2	1.063
			3	1.067
			4	1.073
			5	1.074

tion weigh between 3.4 and 4.1 g and are 99.99% refined. The sample was a disc with a diameter of 20 mm. The weight and shape of the sample were the two factors that determined its thickness. For the purpose of conducting irradiation tests, five samples and 10 monitors made of 99.99% pure niobium foil and 99% pure zirconium, respectively, with the same diameter were fabricated. In forming ZrNb-Te-NbZr, the component sample (Te), monitor (Nb), and zirconium were added. Using the ^{90}Zr(n, $2n$)$^{89m+g}$Zr/^{93}Nb(n, $2n$)^{92m}Nb cross section ratio method, zirconium was irradiated by neutrons to determine the energy of the neutrons, while cadmium foil (with a thickness of ~1 mm) was used to absorb low-energy neutrons and prevent them from irradiating into the sample. This allowed the zirconium to be used to verify the energy of the neutrons. A reduction in the impact of the ^{126}Te(n,γ)^{127m,g}Te reactions on the ^{128}Te(n, $2n$)^{127m,g}Te reactions was observed as a consequence. The data for the reaction cross section of the ^{93}Nb(n, $2n$)^{92m}Nb reaction were obtained from IRDFF-II, 2020 [34]. The details of each sample are displayed in Table 4.

The neutron activation experiment was carried out using a K-400 neutron generator, and the radiation lasted for two to three hours. The neutron yield was calculated to be (4-5)×10^{10} n/s. In the case of deuterium beams, the average energy value was 135 keV, and the average intensity value was 240 μA. At a distance of 5 cm from the sample group, the thickness of the tritium–titanium (T-Ti) was 2.65 mg/cm^2. The experimental setup is shown in Fig. 3. While the experiment was carried out, the fluence variations of the neutrons were monitored using accompanying particles.

B. Calculation of the incident energy of the neutrons

The neutron energies were calculated using [35, 36]

$$(E_n)^{\frac{1}{2}} = \frac{(M_d M_n E_d)^{\frac{1}{2}} \cos\theta \pm (M_d M_n E_d \cos^2\theta + (M_\alpha + M_n)[M_\alpha Q + E_d(M_\alpha - M_n)])^{\frac{1}{2}}}{M_\alpha + M_n}, \tag{4}$$

where E_d denotes the deuteron beam energy; E_n is the kinetic energy of the neutrons emitted at angle θ; and M_d, M_n, and M_α are the masses of the deuteron, neutron, and alpha particles, respectively. At the location of the sample, the uncertainty was calculated using the solid angle of the sample. The neutron energies and their uncertainties are given in Table 5. The results were consistent with the ^{90}Zr(n, $2n$)$^{89m+g}$Zr/^{93}Nb(n, $2n$)^{92m}Nb cross section ratio method (i.e., within the uncertainties).

Table 4. Details of the samples used in this study.

Sample no.	Mass (g)	Thickness (cm)	^{128}Te isotope weight in the sample (g)	Number of target atoms (10^{21} atoms)
1	3.7999	0.1938	1.2061	5.6743
2	3.4459	0.1758	1.0937	5.1457
3	3.6480	0.1861	1.1579	5.4474
4	3.9934	0.2037	1.2675	5.9632
5	4.0404	0.2061	1.2824	6.0334

C. Measurement of radioactivity

The activated sample was monitored using an HPGe detector (ORTEC, model GEM 60P). For ^{60}Co, the detector's efficiency was 68%, and its energy resolution was 1.69 keV at 1.332 MeV. For this experiment, two measurements were taken from each sample. The second dataset was taken 4.7 d later, nearly 12 times the half-life of the ground state of ^{127g}Te, and the first set was taken

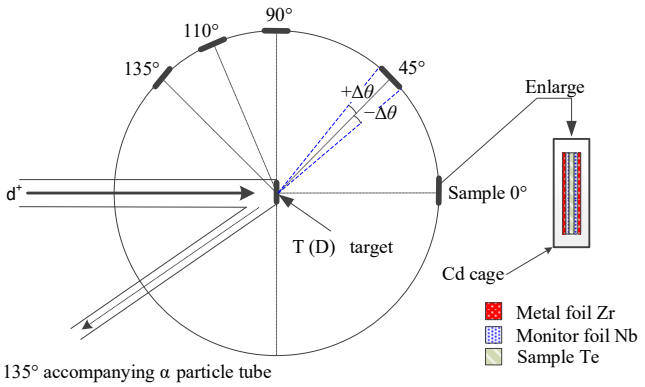

Fig. 3. (color online) Schematic of the experimental setup.

Table 5. Neutron energies as a function of irradiation angle.

Irradiation angle (°)	E_n (MeV)	ΔE_n (MeV @±Δθ)	Neutron energy (MeV)	Uncertainty
135	13.585	$^{-0.094}_{+0.116}$	13.59	0.12
110	13.863	$^{-0.136}_{+0.148}$	13.86	0.15
90	14.129	$^{-0.153}_{+0.155}$	14.13	0.16
45	14.696	$^{-0.124}_{+0.102}$	14.70	0.13
0	14.937	−0.016	14.94	0.02

Table 6. Time factor parameters (in s).

Sample no.	Irradiation T	First measurement		Second measurement	
		Cool t_1	Measurement t_2	Cool t_1	Measurement t_2
1	10860	11056	52526	582178	9063
2	10860	97308	50456	412814	4672
3	10860	64614	32161	417578	9959
4	7200	3618	1608	541419	48809
5	7200	1757	1627	505079	35811

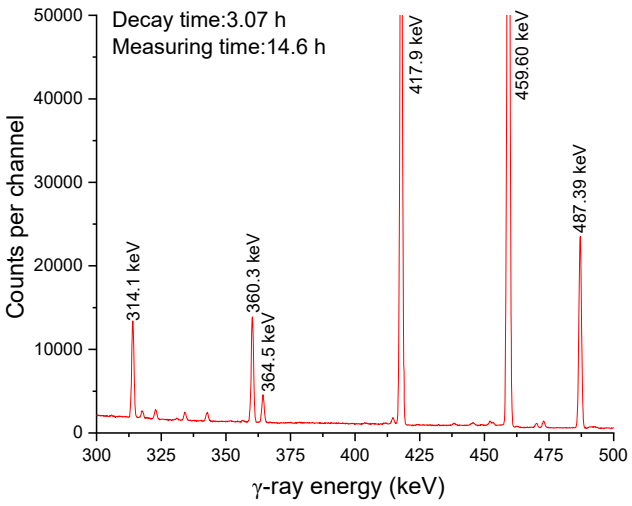

Fig. 4. (color online) Gamma-ray spectrum of the irradiated Te sample approximately 3 h after irradiation.

between 0.5 and 27 h after irradiation. Table 6 displays the specifications of the counting time factor measured in this study. In addition, typical spectra from the irradiated tellurium (Te) samples taken during isomeric and ground state observations are shown in Figs. 4 and 5, respectively. Table 7 presents the half-lives and intensities of the γ-rays used in the analysis. The energy and efficiency were checked by calibrating the detector with reference gamma-ray sources ^{133}Ba, ^{137}Cs, ^{152}Eu, and ^{226}Ra. Further details are available in our previous report [33].

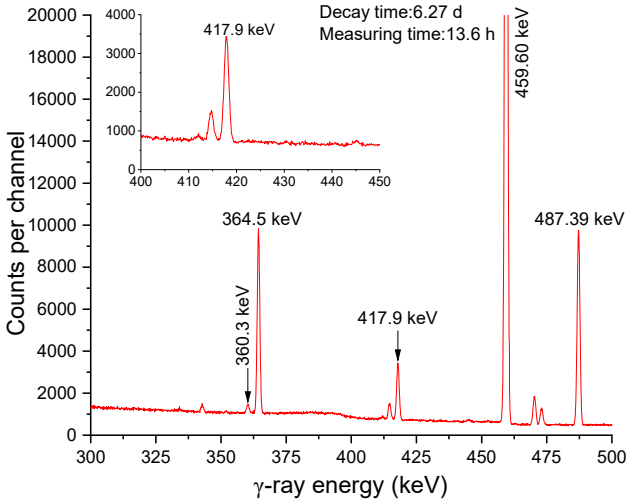

Fig. 5. (color online) Gamma-ray spectrum of the irradiated Te sample approximately 6.27 d after irradiation.

D. Quantification of cross sections and their uncertainty

For the ^{128}Te(n, 2n)^{127m}Te reaction, the neutron-induced cross section (σ_m) was computed using Eq. (1) and the second measurement dataset. When calculating the cross sections for the ^{128}Te(n, 2n)^{127g}Te reaction, the value of C_g in Eq. (3) was determined by subtracting the contribution from ^{127m}Te (as determined via the counting process) from the measured full-energy peak area at 417.9 keV (the ^{127m}Te $\xrightarrow{\text{IT(97.6\%)}}$ ^{127g}Te (counting C^1_{mg}) process). The contributions of the ^{128}Te(n, 2n)^{127m}Te reaction via the isomeric transition (97.6%) were subtracted using [31]

$$C^1_{mg} = \frac{[\varepsilon_g(\lambda_g^2 S_m D_m - \lambda_m^2 S_g D_g)]_{\text{First-measurement}}}{[\varepsilon_g(\lambda_g^2 S_m D_m - \lambda_m^2 S_g D_g)]_{\text{Second-measurement}}} \cdot C^2_{mg}, \quad (5)$$

where counting C^1_{mg} had a cooling time of t_1<27 h and counting C^2_{mg} had a cooling time of t_1>4.7 d.

When the cross sections were determined, there were 14 main sources of uncertainty, the meanings of which are displayed in Table 2. The timing factors are $S_{x,Nb}$ and $D_{x,Nb}$. Because the half-life of the daughter nucleus was relatively long, the contributions of the irradiation, cooling, and measurement times to the uncertainty were negligible. The errors of S and D were calculated using the following formulas:

$$\Delta S = \frac{\mathrm{d}S}{\mathrm{d}T_{1/2}} \times \Delta T_{1/2} = \frac{\mathrm{d}S}{\mathrm{d}\lambda}\frac{\mathrm{d}\lambda}{\mathrm{d}T_{1/2}} \times \Delta T_{1/2}$$
$$= \frac{\mathrm{e}^{-\lambda T} T \lambda}{T_{1/2}} \times \Delta T_{1/2}, \quad (6)$$

Table 7. Decay statistics of nuclear processes caused by neutrons incident on tellurium (Te taken from Hashizume [24]; Nb taken from Baglin [37]).

Reaction	Abundance of target isotope (%)	Half-life of product	*E*-threshold (MeV)	Mode of decay (%)	*E*γ (keV)	*I*γ (%)
^{128}Te(n, 2n) ^{127m}Te	31.74_8	106.1 d_7	8.943	IT(97.60)	88.26	0.084
				β^- (2.40)	57.63	0.51_8
^{128}Te(n, 2n) ^{127g}Te	31.74_8	9.35 h_7	8.854	β^- (100)	**417.9**	0.99_{10}
					360.3	0.135_{10}
^{93}Nb(n, 2n)^{92m}Nb	100	10.15 d_2	8.972	EC (100)	934.46	99.15_4

Uncertainty in the numeric values refers to the last digits of the value: 31.74_8 % means (31.74±0.08)%, 106.1 d_7 means (106.1±0.7) d.

Table 8. Fractional uncertainties (%) of the ^{128}Te(n, 2n)^{127m}Te reaction.

Attributes (x)	Fractional uncertainties (%)				
	13.59 MeV (Δx_i)	13.86 MeV (Δx_j)	14.13 MeV (Δx_k)	14.70 MeV (Δx_l)	14.94 MeV (Δx_n)
C_x	3.8325	3.9749	5.4972	3.1862	3.2701
C_{Nb}	0.9932	0.9856	0.9732	0.8393	0.9720
I_x	10.1010	10.1010	10.1010	10.1010	10.1010
I_{Nb}	0.0403	0.0403	0.0403	0.0403	0.0403
M_x	0.0274	0.0248	0.0290	0.0250	0.0263
M_{Nb}	0.0417	0.1882	0.0410	0.1915	0.0406
η_x	0.2520	0.2520	0.2520	0.2520	0.2520
σ_{Nb}	0.5957	0.5615	0.5461	0.5645	0.5876
ε_x	2.5012	2.5017	2.5012	2.5017	2.5012
ε_{Nb}	2.5031	2.5038	2.5031	2.5038	2.5031
S_x	0.6595	0.6596	0.6595	0.6596	0.6595
S_{Nb}	0.1962	0.1965	0.1962	0.1965	0.1962
D_x	0.6387	0.6337	0.6390	0.6315	0.6305
D_{Nb}	0.1955	0.1959	0.1955	0.1959	0.1955
Total error (%)	11.47	11.52	12.12	11.26	11.29

$$\Delta D = \frac{\mathrm{d}D}{\mathrm{d}T_{1/2}} \times \Delta T_{1/2} = \frac{\mathrm{d}D}{\mathrm{d}\lambda}\frac{\mathrm{d}\lambda}{\mathrm{d}T_{1/2}} \times \Delta T_{1/2} = \frac{[\mathrm{e}^{-\lambda t_1} t_1 - \mathrm{e}^{-\lambda(t_1+t_2)}(t_1+t_2)]\lambda}{T_{1/2}} \times \Delta T_{1/2}. \quad (7)$$

The total section uncertainty was calculated using the sum of squares formula [8, 38–40]. Tables 8 and 9 show the fractional uncertainties in the factors that affected the reaction cross section. The covariance matrix was dispersed between neutron energies. After calculating the fractional uncertainties, covariance analysis was used to generate correlation coefficients between the energy attributes. Table 10 presents the correlation coefficients between certain characteristics and energies, where i, j, k, l, and n indicate 13.59, 13.86, 14.13, 14.70, and 14.94 MeV, respectively. To calculate (σ_{xi},σ_{xj}), 14 subsets (attributes) were added and used in the following equation [39]:

$$\mathrm{Cov}\left(\sigma_{xi'}\sigma_{xj}\right) = \sum_i \sum_j \Delta x_i \times \mathrm{Cor}\left(\Delta x_i, \Delta x_j\right) \times \Delta x_j. \quad (8)$$

Using Eq. (8), a [5×5] covariance matrix was created. The overall uncertainty in the measured cross section was calculated using [39]

$$\mathrm{Cov}\left(\sigma_{xi}, \sigma_{xi}\right) = \left(\Delta\sigma_{xi}\right)^2. \quad (9)$$

Based on the total uncertainty and covariance matrix, the correlation matrix [5×5] between neutron energies was propagated using [39]

$$\mathrm{Cor}\left(\sigma_{xi}\sigma_{xj}\right) = \frac{\mathrm{Cov}\left(\sigma_{xi}\sigma_{xj}\right)}{\left(\Delta\sigma_{xi}\right)\cdot\left(\Delta\sigma_{xj}\right)}. \quad (10)$$

Tables 11 and 12 provide the measured cross sections, uncertainties, and correlation matrices of the ^{128}Te(n, 2n)^{127m,g}Te reaction. Table 13 shows the experimentally observed neutron energy-dependent ^{128}Te(n, 2n)$^{127(m+g)}$Te

Table 9. Fractional uncertainties (%) of the ^{128}Te(n, 2n)^{127g}Te reaction.

Attributes (x)	Fractional uncertainties (%)				
	13.59 MeV (Δx_i)	13.86 MeV (Δx_j)	14.13 MeV (Δx_k)	14.70 MeV (Δx_l)	14.94 MeV (Δx_n)
C_x	0.1681	2.9452	0.2126	1.5636	0.1317
C_{Nb}	0.9932	0.9856	0.9732	0.8393	0.9720
I_x	10.1010	10.1010	10.1010	10.1010	10.1010
I_{Nb}	0.0403	0.0403	0.0403	0.0403	0.0403
M_x	0.0274	0.0248	0.0290	0.0250	0.0263
M_{Nb}	0.0417	0.1882	0.0410	0.1915	0.0406
η_x	0.2520	0.2520	0.2520	0.2520	0.2520
σ_{Nb}	0.5957	0.5615	0.5461	0.5645	0.5876
ε_x	2.5012	2.5017	2.5012	2.5017	2.5012
ε_{Nb}	2.5031	2.5038	2.5031	2.5038	2.5031
S_x	0.6681	0.6945	0.6681	0.6945	0.6681
S_{Nb}	0.1962	0.1965	0.1962	0.1965	0.1962
D_x	0.4682	0.7091	1.0743	0.6806	0.2449
D_{Nb}	0.1955	0.1959	0.1955	0.1959	0.1955
Total error (%)	10.80	11.21	10.84	10.92	10.79

Table 10. Correlation coefficients of several parameters in the 13–15 MeV range for the ^{128}Te(n, 2n)^{127m,g}Te reaction cross section. At these energies, there is a full correlation between the I_x, I_{Nb}, η_x, σ_{Nb}, ε_{Nb}, $S_{Nb,}$ and D_{Nb} subsets.

Cor(Δx, Δx)	Correlation coefficient (Δx, Δx)						
	C_x	C_{Nb}	M_x	M_{Nb}	ε_x	S_x	D_x
(Δx_i, Δx_i)	1	1	1	1	1	1	1
(Δx_i, Δx_j)	0	0	0	0	0.9994	0	0
(Δx_i, Δx_k)	0	0	0	0	0.9994	0	0
(Δx_i, Δx_l)	0	0	0	0	0.9994	0	0
(Δx_i, Δx_n)	0	0	0	0	0.9994	0	0
(Δx_j, Δx_j)	1	1	1	1	1	1	1
(Δx_j, Δx_k)	0	0	0	0	0.9994	0	0
(Δx_j, Δx_l)	0	0	0	0	0.9994	0	0
(Δx_j, Δx_n)	0	0	0	0	0.9994	0	0
(Δx_k, Δ_k)	1	1	1	1	1	1	1
(Δx_k, Δx_l)	0	0	0	0	0.9994	0	0
(Δx_k, Δx_n)	0	0	0	0	0.9994	0	0
(Δx_l, Δx_l)	1	1	1	1	1	1	1
(Δx_l, Δx_n)	0	0	0	0	0.9994	0	0
(Δx_n, Δx_n)	1	1	1	1	1	1	1

reaction cross sections and isomeric ratios.

IV. CALCULATION OF NUCLEAR MODEL-BASED CROSS SECTIONS

TALYS (version 1.96) was used to calculate the ^{128}Te(n, 2n)^{127m,g}Te reaction cross sections and isomeric ratio [25]. TALYS simulates nuclear reaction cross sections from the reaction threshold up to 200 MeV, and it analyzes and predicts nuclear reactions worldwide using cutting-edge nuclear structure and reaction models [41]. The reaction mechanism is described using the optical

Table 11. Experimental cross sections, total uncertainties, and correlation matrices for the ^{128}Te(n, 2n)^{127m}Te reaction.

Neutron energy E_n (MeV)	Cross section σ_x (mb)	$\Delta\sigma_x$ (%)	Correlation matrix				
13.59±0.12	887±102	11.47	1.0000				
13.86±0.15	923±106	11.52	0.8707	1.0000			
14.13±0.16	959±116	12.12	0.8270	0.8235	1.0000		
14.70±0.13	1006±113	11.26	0.8908	0.8870	0.8425	1.0000	
14.94±0.02	1028±116	11.29	0.8882	0.8844	0.8400	0.9048	1.0000

Table 12. Experimental cross sections, total uncertainties, and correlation matrices for the ^{128}Te(n, 2n)^{127g}Te reaction.

Neutron energy E_n (MeV)	Cross section σ_x (mb)	$\Delta\sigma_x$ (%)	Correlation matrix				
13.59±0.12	579±63	10.80	1.0000				
13.86±0.15	588±66	11.21	0.9497	1.0000			
14.13±0.16	579±63	10.84	0.9817	0.9460	1.0000		
14.70±0.13	544±59	10.92	0.9754	0.9399	0.9716	1.0000	
14.94±0.02	543±59	10.79	0.9864	0.9505	0.9826	0.9763	1.0000

Table 13. Isomeric ratios (IRs) experimental cross sections (CSs) for the ^{128}Te(n, 2n)$^{127(m+g)}$Te reaction.

E_n (MeV)	This study		Monitor reaction ^{93}Nb(n, 2n)^{92m}Nb	
	CS (mb)	IR (σ_m/σ_g)	CS (mb)	Reference
13.59±0.12	1466±119	1.53±0.24	454.55±2.71	[34]
13.86±0.15	1511±125	1.57±0.25	457.99±2.57	[34]
14.13±0.16	1538±132	1.66±0.27	459.76±2.51	[34]
14.70±0.13	1550±128	1.85±0.29	460.17±2.60	[34]
14.94±0.02	1571±130	1.89±0.30	460.28±2.70	[34]

model potential (OMP), direct reactions included in the distorted wave Born approximation (DWBA), and compound nucleus model. To run the simulations, the ECIS-06 code in TALYS is used. Furthermore, pre-equilibrium reactions are modeled using both classical and quantum mechanical techniques. Masses, discrete levels, level densities, photon strength functions, and fission barriers are the most important nuclear structure models. In summary, the TALYS software is designed to provide a comprehensive description of the observables associated with nuclear reactions. It is also intended to serve as an essential link between the fundamentals of nuclear physics and its applications.

V. DISCUSSIONS

Tables 11–13 display the cross sections determined in this study. The characteristic ray intensity of the ^{127g}Te daughter nucleus had an uncertainty of 10.10%, which resulted in insignificant measurements. Similarly, the excited and ground state cross sections were uncertain in a range of 10.8%-12.2%. The minimal contribution of the ^{126}Te(n,γ) reaction products to the γ-ray activity could be disregarded because the reaction had a small cross section at the neutron energy of 14 MeV. Cadmium foil was used to decrease the heat and epithermal neutron impacts on the samples. The results for each reaction, as well as the isomeric cross section ratio, are described in the rest of this section.

A. ^{128}Te(n, 2n)^{127m}Te reaction

Four previous cross-sectional experimental studies have examined the ^{128}Te(n, 2n)^{127m}Te reaction, in which the product has a half-life of 105–109 days. Lu and Zhou utilized typical gamma rays of 417 and 360.3 keV, respectively, while Husain and Kuroda [13] and Lu *et al.* [12] only gathered data at a single neutron energy point. According to the data presented in Fig. 1, the 417.9-keV and 360.3-keV lines do not correspond to the characteristic ray of ^{127m}Te, but rather represent the characteristic γ-ray of its ground state. This experiment used the strongest characteristic ray of ^{127g}Te (417 keV) to study the excited state cross section of the ^{128}Te(n, 2n)^{127m}Te reaction. We did not investigate the decay of ^{127g}Te via 417.9-keV γ-

rays for the first 4.7 days, but after the irradiation, the decay was due to interference from the ^{128}Te(n, 2n)^{127g}Te reaction. When the cooling time reached more than 12 times the half-life of the ground state, the ground state characteristic 417.9-keV gamma-ray count could be considered to originate entirely from the path $^{128}\mathrm{Te}(n,2n)^{127m}\mathrm{Te} \xrightarrow{\mathrm{IT}(97.6\%)} {}^{127g}\mathrm{Te}(\beta^-)$, allowing the cross section of the nuclear reaction ^{128}Te(n, 2n)^{127m}Te to be calculated. Figure 6 displays the theoretical excitation function and experimental cross sections found for the ^{128}Te(n, 2n)^{127m}Te reaction, including the cross section derived in this study. The latter exhibited a considerable increase as the neutron energy increased. This trend matches the TALYS-1.96 theoretical results. The data produced by Lu *et al.* [12], Bomann *et al.* [14], and ldmodels 3, 4, and 6 in Talys-1.96 are in agreement with the data produced by this study between 13 and 15 MeV, but the data by Husain and Kuroda [13] are roughly 80% lower.

B. ^{128}Te(n, 2n)^{127g}Te reaction

Eleven previous studies gathered cross section data for the ^{128}Te(n, 2n)^{127g}Te reaction [12–14,16-23]. Table 1 shows that six of these studies used gamma counting and two studies used beta counting, and the rest did not provide experimental information (see Table 1). Most early studies employed GeLi and NaI detectors with poor energy resolution. However, rays of similar energy are also influenced near the 417-keV peak based on the gamma-ray spectrum obtained (Figs. 4 and 5). Detectors with less-than-perfect resolution may be indistinguishable. Early experimental results ranged from 240 to 840 mb and were quite distinct. This study used 417.9-keV γ-rays (I_γ=0.99%) emitted during the ^{127g}Te decay to calculate the reaction cross section of ^{128}Te(n, 2n)^{127g}Te. All γ-ray spectrum acquisitions were cooled within 27 h. When computing the ground state cross section using Eq. (3), Eq. (5) subtracts the excited state contribution. Figure 7 depicts the data produced by this study and those produced by the Refs. [14–22] for the ^{128}Te(n, 2n)^{127g}Te reactions along with the TALYS-1.96 computations generated using ldmodels 1-6 (continuous lines). The values obtained in this study are consistent with those of previous reports [16, 18, 19, 21] within the experimental uncertainties in the 13–15 MeV range. However, Majumdar and Chatterjee [22] reported data that were 100% lower than ours, while the result produced by Bormann *et al.* [14] was about 300 millitargets higher. Paul and Clarke [20] give a value of 779±234 mb, with an uncertainty of 30%. The substantial disparities may be due to different excited state deduction procedures. Thus far, researchers [15] have reported the formation cross sections for the excited state, but not for the ground state.

C. ^{128}Te(n, 2n)$^{127(m+g)}$Te reaction

Figure 8 presents the theoretical predictions for the

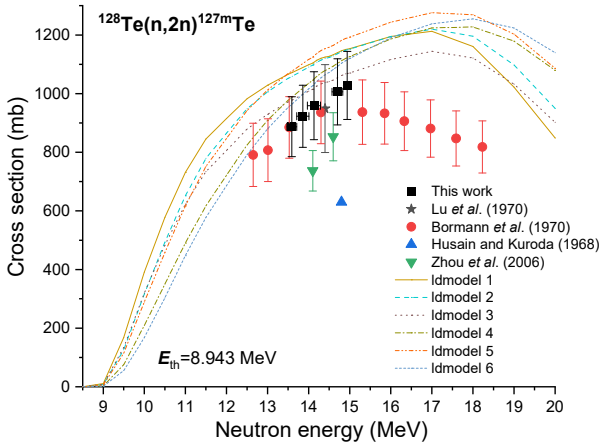

Fig. 6. (color online) Comparison between the excitation function of the ^{128}Te(n, 2n)^{127m}Te reactions and the experimental data reported for the cross section, including those produced by this study.

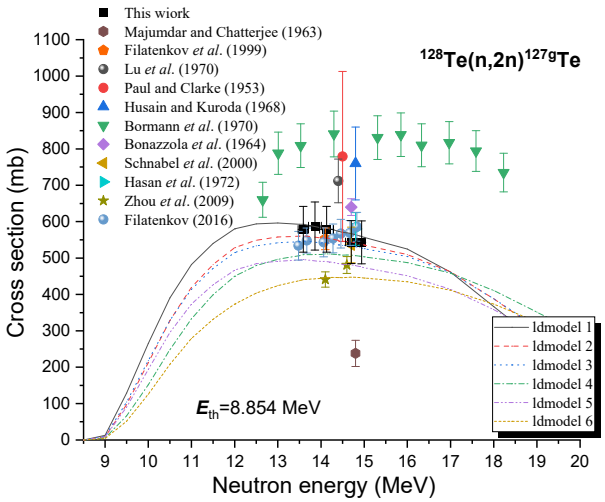

Fig. 7. (color online) Comparison between the excitation function of the ^{128}Te(n, 2n)^{127g}Te reactions and the experimental data reported for the cross section, including those produced by this study.

^{128}Te(n, 2n)$^{127(m+g)}$Te reaction generated using statistical models and databases, as well as the cross section data produced by this study and by Refs. [12–14]. We found that within the experimental uncertainty, the results obtained in this study in the 13–15 MeV range agree well with previously reported data [12–14] and the TENDL–2021 predictions [30]. However, the findings of Bomann *et al.* [14], as well as the TALYS-1.96 calculations that utilize ldmodel 1 (with the constant temperature and Fermi gas model), exhibit higher values compared to those reported by Husain and Kuroda [13]. The evaluation data from databases such as ENDF/B-VIII.0 [26], BROND-3.1 [27], and JENDL-5 [29] further support these results.

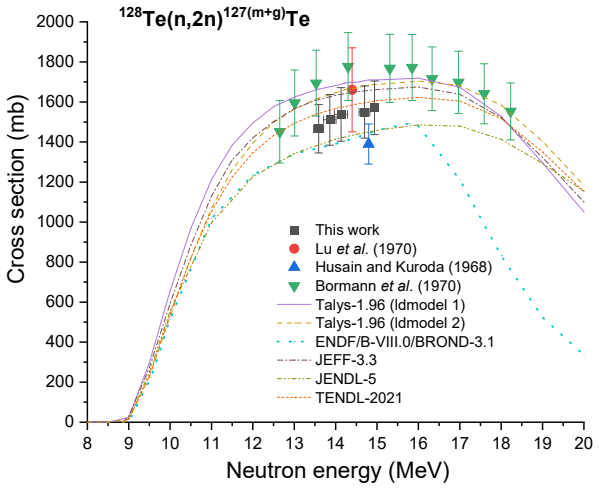

Fig. 8. (color online) Excitation function of the ^{128}Te(n, $2n$)$^{127(m+g)}$Te reaction.

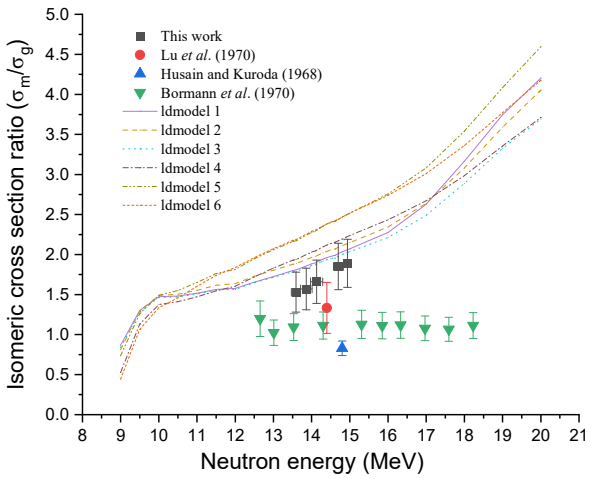

Fig. 9. (color online) Isomeric cross section ratio for the ^{128}Te(n, $2n$)^{127m}Te and ^{128}Te(n, $2n$)^{127g}Te reactions as a function of the neutron energy.

D. Isomeric cross section ratio

We determined the isomeric cross section ratio σ_m/σ_g for the ^{127m,g}Te pair formed during the (n, $2n$) reaction on ^{128}Te. Based on the findings, the isomeric cross section ratio for neutron energies of 13.59±0.12, 13.86±0.15, 14.13±0.16, 14.70±0.13, and 14.94±0.02 MeV was 1.53±0.24, 1.57±0.25, 1.66±0.27, 1.85±0.29, and 1.89±0.30, respectively. The findings of the experiments and the theoretical calculations performed by TALYS-1.96 are presented in Fig. 9. As can be seen from Fig. 9, our data are consistent with the data of Lu *et al.* [12], but higher than the results of Husain and Kuroda [13] and Bomann *et al.* [14]. This inconsistency was primarily caused by the inconsistent decay data used in the experiment and/or the different methods used to deal with the interference reaction. The isomeric cross section ratio derived in this study exhibited a modest increase with increasing neutron energy, which is an important finding. In general, in the 14-MeV neutron energy region, the excited state cross section of the (n, $2n$) reaction increased as the incident neutron energy increased, while the ground state cross section of the (n, $2n$) reaction decreased or increased slowly as the neutron energy increased. According to this effect, the synthesis of the high-spin isomer ($11/2^{-}\rightarrow 3/2^{+}$) was favored at higher excitation energies. This phenomenon is also found in other neutron- and charged particle-induced reactions that occur close to the threshold values [42–44]. The isomeric cross section ratio increased between 13 and 15 MeV for each of the six individual ldmodels.

VI. CONCLUSIONS

In this study, secondary nuclear decay was used to measure the cross section of the nuclear reaction ^{128}Te(n, $2n$)^{127m}Te. The activation method was used to obtain the cross sections of the ^{128}Te(n, $2n$)^{127m,g}Te reactions and the isomeric cross section ratio σ_m/σ_g of ^{127m,g}Te at five neutron energies ranging from 13 to 15 MeV. The theoretical nuclear model software TALYS-1.96 was utilized to estimate the excitation function of the neutron energy threshold up to 20 MeV according to six ldmodels. The experimental and theoretically calculated data were compared to the measurement results. We concluded that the difference between the decay data, reasonable disposal of interference reactions, and reasonable arrangement of secondary nuclear decay time factors determined the discrete measurement results, such as the half-life and characteristic gamma-ray intensity. To obtain high-precision cross section data, it was necessary to ensure that these characteristics were accurate. Hence, the new data obtained in this study for the cross sections and isomeric cross section ratio of the nuclear reactions ^{128}Te(n, $2n$)^{127m,g}Te are essential for testing nuclear models and determining the crucial parameters.

ACKNOWLEDGEMENTS

We would like to thank the Intense Neutron Generator group at the Chinese Academy of Engineering Physics for performing the irradiations.

References

[1] J. Luo and L. Jiang, Chin. Phys. C, **44**, 114002 (2020)
[2] L. He, J. Luo, L. Jiang, Chin. Phys. C, **47**, 034001 (2023)
[3] J. Luo, L. Jiang, J. Liang, *et al.*, Chin. Phys. C, **46**, 044001 (2022)
[4] J. Tang, Q. An, J. Bai *et al.*, Nucl. Sci. Tech. **32**, 11 (2021)
[5] A. Rodrigo, N. Otuka, S. Takács *et al.*, Atomic Data and

Nuclear Data Tables **153**, 101583 (2023)
[6] J. Luo, J. Liang, L. Jiang *et al*., Nucl. Sci. Tech. **34**, 4 (2023)
[7] C. Lan, Y. Niu, Y. Wei *et al*., Chin. Phys. C, **47**, 094001 (2023)
[8] A. Gandhi, Aman Sharma, Rebecca Pachuau *et al*., Chin. Phys. C, **46**, 014002 (2022)
[9] J. Luo and L. Jiang, Eur. Phys. A, **56**, 125 (2020)
[10] L. Liu, Y. Liu, X. Huang *et al*., Phys. Rev. C, **109**, 014603 (2024)
[11] S. Sudára and S. M. Qaim, Nucl. Phys. A, **979**, 113 (2018)
[12] W. D. Lu, N. Ranakumar, R. W. Fink, Phys. Rev. C, **1**, 350 (1970)
[13] L. Husain and P. K. Kuroda, Nucl. Phys. A, **114**, 663 (1968)
[14] M. Bormann, H. H. Bissem, E. Magiera, *et al*., Nucl. Phys. A, **157**, 481 (1970)
[15] F. Zhou, Y. Zhang, F. Tuo *et al*., Appl. Radiat. Isot. **64**, 815 (2006)
[16] C. Schnabel, I. Leya, R. Michel *et al*., Radiochim. Acta **88**, 439 (2000)
[17] F. Zhou, L. Gao, X. Kong *et al*., Phys. Rev. C, **80**, 054615 (2009)
[18] A. A. Filatenkov, S. V. Chuvaev, V. A. Yakovlev *et al*. , Report, Khlopin Radiev. Inst. , Leningrad Reports; No. 252, 1999
[19] A. A. Filatenkov, Report, USSR report to the I. N. D. C. ; No. 0460, 2016
[20] E. B. Paul and R. L. Clarke, Can. J. Phys. **31**, 267 (1953)
[21] S. S. Hasan, R. Prasad, and M. L. Sehgal, Nucl. Phys. A, **181**, 101 (1972)
[22] N. K. Majumdar and A. Chatterjee, Nucl. Phys. **41**, 192 (1963)
[23] G. C. Bonazzola, P. Brovetto, E. Chiavassa *et al*., Nucl. Phys. **51**, 337 (1964)
[24] A. Hashizume, Nucl. Data Sheets **112**, 1647 (2011)
[25] A. J. Koning, S. Hilaire, S. Goriely, "TALYS-1.96, A nuclear reaction program, " NRG-1755 ZG Petten, The Netherlands, 2021, http://www.talys.eu
[26] ENDF/B-VIII. 0 (USA, 2018), Evaluated Nuclear Data File (ENDF) Database Version of 2023-08-25. https://www-nds.iaea.org/exfor/endf.htm
[27] BROND-3.1 (Russia, 2016), Evaluated Nuclear Data File (ENDF) Database Version of 2023-08-25. https://www-nds.iaea.org/exfor/endf.htm
[28] JEFF-3.3 (Europe, 2017), Evaluated Nuclear Data File (ENDF) Database Version of 2023-08-25. https://www-nds.iaea.org/exfor/endf.htm
[29] JENDL-5 (Japan, 2021), Evaluated Nuclear Data File (ENDF) Database Version of 2023-08-25. https://www-nds.iaea.org/exfor/endf.htm
[30] TENDL-2019 (TALYS, 2019) , Evaluated Nuclear Data File (ENDF) Database Version of 2023-08-25. https://www-nds.iaea.org/exfor/endf.htm
[31] J. Luo, L. Jiang, L. He *et al*., Radiat. Phys. Chem. **206**, 110759 (2023)
[32] J. Luo and L. Jiang, Eur. Phys. A, **55**: 27 (2019)
[33] J. Luo, J. Liang, L. Jiang *et al*., Eur. Phys. A, **58**, 142 (2022)
[34] IRDFF-II, 2020. International Reactor Dosimetry and Fusion File, January. https://www-nds.iaea.org/IRDFF/
[35] J. Luo, J. Liu, J. Han *et al*., Radiat. Phys. Chem. **92**, 28 (2013)
[36] J. Luo, R. Liu, L. Jiang *et al*., Radiat. Phys. Chem. **79**, 1169 (2010)
[37] Coral M. Baglin, Nucl. Data Sheets **113**, 2187 (2012)
[38] N. Otuka, B. Lalremruata, M. U. Khandaker *et al*., Radiat. Phys. Chem. **140**, 502 (2017)
[39] A. Gandhi, A. Sharma, A. Kumar *et al*., Phys. Rev. C, **102**, 014603 (2020)
[40] Akash Hingu, S. Mukherjee, Siddharth Parashari *et al*., Chin. Phys. C, **48**, 024001 (2024)
[41] A. J. Koning, S. Hilaire, and S. Goriely, Eur. Phys. A, **59**, 131 (2023)
[42] C. D. Nesaraja, S. Sudár, and S. M. Qaim, Phys. Rev. C, **68**, 024603 (2003)
[43] S. Sudár and S. M. Qaim, Phys. Rev. C, **73**, 034613 (2006)
[44] M. Al-Abyad, S. Sudár, M. N. H. Comsan *et al*., Phys. Rev. C, **73**, 064608 (2006)